Published in final edited form as:
Cell Metab. 2013 September 3; 18(3): 403–415. doi:10.1016/j.cmet.2013.08.011.

DNA damage triggers a chronic auto-inflammatory response leading to fat depletion in NER progeria

Ismene Karakasilioti[1,2], **Irene Kamileri**[1,2], **Georgia Chatzinikolaou**[1], **Theodoros Kosteas**[1], **Eleni Vergadi**[3], **Andria Rasile Robinson**[4], **Iannis Tsamardinos**[5,6], **Tania A Rozgaja**[7], **Sandra Siakouli**[2], **Christos Tsatsanis**[3], **Laura J. Niedernhofer**[4,7,8], and **George A. Garinis**[1,2,*]

[1]Institute of Molecular Biology and Biotechnology, Foundation for Research and Technology-Hellas, GR70013, Heraklion, Crete, Greece

[2]Department of Biology, University of Crete, Heraklion, Crete, Greece

[3]Department of Clinical Chemistry, School of Medicine, University of Crete Heraklion, Greece

[4]University of Pittsburgh Cancer Institute, Pittsburgh, Pennsylvania, USA

[5]Department of Computer Sciences, University of Crete, Heraklion GR71409, Greece

[6]Bioinformatics Laboratory, Institute of Computer Science, Foundation for Research and Technology-Hellas, GR70013, Heraklion, Crete, Greece

[7]Department of Metabolism & Aging, The Scripps Research Institute, Florida, 130 Scripps Way, 3B3, Jupiter, FL 33458

[8]Department of Microbiology and Molecular Genetics, University of Pittsburgh School of Medicine, Pittsburgh, Pennsylvania, USA

Abstract

Lipodystrophies represent a group of heterogeneous disorders characterized by loss of fat tissue. However, the underlying mechanisms remain poorly understood. Using mice carrying an ERCC1-XPF DNA repair defect systematically or in adipocytes, we show that DNA damage signaling triggers a chronic auto-inflammatory response leading to fat depletion. *Ercc1*$^{-/-}$ and aP2-*Ercc1*$^{f/-}$ fat depots show extensive gene expression similarities to lipodystrophic *Ppar*$\gamma^{ldi/+}$ animals along with focal areas of ruptured basement membrane, the reappearance of primary cilia, necrosis, fibrosis and a marked decrease in adiposity. We find that persistent DNA damage in aP2-*Ercc1*$^{f/-}$ fat depots and in adipocytes *ex vivo* trigger the induction of pro-inflammatory factors by promoting transcriptionally active histone marks and the dissociation of nuclear receptor co-repressor complexes from promoters; the response is cell-autonomous and requires ATM. Thus, persistent DNA damage-driven auto-inflammation plays a causative role in adipose tissue degeneration with important ramifications for progressive lipodystrophies and natural aging.

Keywords

DNA damage; Nucleotide Excision Repair; Chronic Inflammation; Adipose tissue

*Corresponding author: George A. Garinis (garinis@imbb.forth.gr).

Introduction

In humans, the causative role of DNA damage in age-related diseases is supported by several premature aging-like (progeroid) disorders with defects in DNA repair (Kamileri et al., 2012a; Schumacher et al., 2009). Nucleotide excision repair (NER) represents one such pathway that operates via a “cut and patch” mechanism and proceeds in successive steps beginning with lesion recognition, unwinding of the double helix at damaged DNA sites and lesion verification followed by excision of the DNA damage and gap-filling DNA synthesis (Kamileri et al., 2012a). NER is divided into two sub-pathways, global genome repair (GGR) and transcription-coupled repair (TCR); differing primarily in how the damage is initially recognized (Hanawalt, 2002). In humans, defects in GGR cause the cancer-prone syndrome xeroderma pigmentosum (XP, complementation groups XP-A to XP-G) (DiGiovanna and Kraemer, 2012). Instead, defects in TCR give rise to a heterogeneous group of progeroid syndromes, including the Cockayne syndrome (CS), trichothiodystrophy (TTD) or XFE(Kamileri et al., 2012a). CS, TTD and XFE patients are characterized by postnatal growth failure, skeletal and neuronal abnormalities, depletion of subcutaneous fat depots and short lifespan, but not cancer (Garinis et al., 2008; Kamileri et al., 2012a).

Whereas genome instability has been established as the underlying cause of mutations leading to increased skin cancer predisposition in XP, the functional links between defective NER and the manifestation of progeroid or developmental defects remain obscure (Kamileri et al., 2012a). Using ERCC1-defective animal models of a human progeroid syndrome (Niedernhofer et al., 2006), we provide evidence for a causal link between persistent DNA damage and the gradual manifestation of progressive lipodystrophy in NER progerias; we find that the accumulation of irreparable DNA inter-strand crosslinks (ICLs) triggers the transcriptional derepression of pro-inflammatory cytokines in adipocytes, the recruitment of leukocytes to sites of tissue damage and the destruction of white adipose tissue depots in NER-defective animals. Taken together, our findings provide a mechanism by which stochastic, endogenous DNA damage instigates tissue-specific pathology in progeroid syndromes and by analogy likely with aging.

Results

Loss of adipose tissue in (aP2-*Cre*) *Ercc1*$^{-/-}$ animals

Besides dwarfism, CS, TTD and XFE patients are characterized by loss of subcutaneous fat, which is also seen with normal aging (Sepe et al., 2011). To gain greater understanding into the role of unrepaired DNA damage in adipose tissue degeneration, we compared the white (WAT) and brown (BAT) adipose fat depots from *Ercc1*$^{-/-}$ mice and animals in which *Ercc1* is knocked-out in the fat, causing impaired DNA repair systemically or in adipose tissue, respectively. Beginning postnatal day 5 (P5), *Ercc1*$^{-/-}$ animals fail to gain weight and display gradual reduction in epididymal, cervical, interscapular and subcutaneous WAT depots. P15 *Ercc1*$^{-/-}$ mice show a ~50% decrease in epididymal WAT with most P20 *Ercc1*$^{-/-}$ mice having few or no residual WAT depots with a small -albeit not significant- reduction of BAT depots (Figure 1A and S1A–B). *Ercc1*$^{-/-}$ mice are growth-defective, show premature aging features in several organs and die within a month after birth of liver

failure (Niedernhofer et al., 2006; Selfridge et al., 2001). To test whether fat depletion in *Ercc1*$^{-/-}$ mice is the consequence of defects in other tissues or is cell-autonomous, we intercrossed animals homozygous for the floxed *Ercc1* allele (*Ercc1*$^{F/F}$) (Verhagen-Oldenampsen et al., 2012) with those carrying the adipose protein 2 (aP2)-*Cre* transgene in an *Ercc1* heterozygous background; aP2 is a carrier protein for fatty acids that is primarily expressed in adipocytes (Jones et al., 2005). Crossing the aP2 with Rosa YFP transgenic animals confirmed the specificity of aP2-driven YFP expression to adipocytes at P30 (Figure 1B; **upper panel**) but not at P15 (Figure S1O), the cell type-specific ablation of *Ercc1* in 1.5-month old aP2-*Ercc1*$^{F/-}$ WAT depots (Figure 1B; **lower panel and** Figure S1I) and the normative ERCC1 expression levels in aP2-*Ercc1*$^{F/-}$ organs other than the adipose tissue (Figure S1C and S1K–L). Excision of the floxed *Ercc1* allele was further confirmed by genomic PCR amplification on DNA derived from aP2-*Ercc1*$^{F/+}$ and aP2-*Ercc1*$^{F/-}$ adipose tissues (Figure S1F–G) as well as the significant decrease in the *Ercc1* mRNA levels in 45-day old aP2-*Ercc1*$^{F/-}$ adipose WAT depots (Figure S1H). aP2-*Ercc1*$^{F/-}$ mice were born at the expected Mendelian frequency and showed no developmental defects or other pathological features, including any visible defects in adipose tissue; the mRNA levels of *Fabp4* and *Adiponectin*, an adipocyte secretory adipokine previously linked to insulin resistance and diabetes (Kadowaki et al., 2006), were comparable between 1.5-month old aP2-*Ercc1*$^{F/-}$ WAT tissues and control animals (Figure S1J). Beginning at 2.5 months, aP2-*Ercc1*$^{F/-}$ animals show a slow but steady loss of epididymal, interscapular and subcutaneous fat depots (Figure 1C and S1D) resulting in a ~30% reduction in body weight (Figure 1D), a >50% reduction in epididymis WAT (Figure 1E) and interscapular BAT depots (Figure S1N); the weight of other organs was comparable to that of control animals (Figure S1E). Unlike the 1.5-month old aP2-*Ercc1*$^{F/-}$ animals, computer image analysis revealed substantial differences in the number and size of adipocytes of 4-month old aP2-*Ercc1*$^{F/-}$ animals compared to age-matched controls (Figure 1F). Thus, adult mice lacking ERCC1 specifically in the adipose tissue exhibit marked WAT and BAT abnormalities; importantly, both adipose tissue depots develop normally in these mice with defects gradually appearing at later stages in life.

Morphological changes in *Ercc1*$^{-/-}$ and aP2-*Ercc1*$^{F/-}$ adipose tissue depots and aP2-*Ercc1*$^{F/-}$ metabolic abnormalities

Oil Red O staining of 4-month old aP2-*Ercc1*$^{F/-}$ tissues revealed accumulation of triglycerides in heart and muscle (Figure 1G), but not in liver, kidney or spleen (Figure S2A). The 4-month old aP2-*Ercc1*$^{F/-}$ had normal serum cholesterol levels, a significant increase in triglycerides, not seen in 1.5-month old mice (Figure S2B–C) and decreased adiponectin protein levels both in serum and WAT as compared to aP2-*Ercc1*$^{F/+}$ control mice (Figure 2A and S2C). Prior to the glucose and insulin tolerance test, 4-month old aP2-*Ercc1*$^{F/-}$ animals had basal plasma glucose levels comparable to wild-type mice after a 5 hour fast (Figure 2B and S2D). Upon intraperitoneal glucose infusion, the 4-month old but not the 1.5-month old aP2-*Ercc1*$^{F/}$ mice had increased plasma glucose levels compared to controls (Figure 2B and S2E). Staining of pancreata from fasted aP2-*Ercc1*$^{F/-}$ mice and measurement of serum insulin levels revealed increased number and size of insulin foci and hyperinsulinaemia respectively compared to aP2-*Ercc1*$^{F/+}$ controls (Figure 2C–D and S2F–G). aP2-*Ercc1*$^{F/-}$ and aP2-*Ercc1*$^{F/+}$ animals had comparable serum glucose levels following

intraperitoneal insulin infusion (Figure S2D). Food and water intake measurements in 2.5 month old aP2-*Ercc1*$^{F/-}$ and aP2-*Ercc1*$^{F/+}$ animals over a period of 30 days revealed no significant differences (Figure S2H). Thus, similar to other lipodystrophic animal models, the aP2-*Ercc1*$^{F/-}$ animals exhibit metabolic abnormalities that are associated with type II diabetes mellitus.

Scanning electron microscopy of epididymal WAT and BAT derived from 15-day old *Ercc1*$^{-/-}$ and wt animals revealed no apparent differences (Figure 2E and S2I). Both *Ercc1*$^{-/-}$ and wt adipose depots, show areas of dense cilia formation characteristic of adipogenic differentiation during development (Satir et al., 2010) (Figure 2E; embedded magnification). Likewise, the 1.5-month old aP2-*Ercc1*$^{F/-}$ and aP2-*Ercc1*$^{F/+}$ white adipocytes appeared healthy with spherical and unilocular lipid depots (Figure 2F; **as shown**). In contrast, the WAT of 4-month old aP2-*Ercc1*$^{F/-}$ animals showed focal areas of ruptured basal membrane (Figure 2F-i) and frequent loss of adipocytes (Figure 2F-ii); red blood cells were sporadically found to occupy empty adipocyte cavities, likely marking the former presence of adipocyte-associated capillaries (Figure 2F-ii; embedded magnification). Staining with Platelet/Endothelial Cell Adhesion Molecule 1 (PECAM-1) revealed a dense and well-structured vasculature in aP2-*Ercc1*$^{F/-}$ WAT samples compared to controls (Figure S2L). We also found areas of cilia recurrence in the WAT of 4-month old aP2-*Ercc1*$^{F/-}$ animals (Figure 2F-iii; embedded magnification). None of these pathological features were seen in the 4-month old aP2-*Ercc1*$^{F/+}$ WAT depots (Figure S2J). Unlike the aP2-*Ercc1*$^{F/+}$ controls (Figure S2I–J), we noticed the presence of excessive interstitial fibrosis at sites of tissue damage in 4-month old aP2-*Ercc1*$^{F/-}$ animals (Figure 2F-iv and 2G). Together, these findings resemble the pathological abnormalities seen in progressive lipodystrophies ultimately leading to severe metabolic and physiologic abnormalities (Hegele et al., 2007).

Transcriptome analysis of epididymal WAT depots in *Ercc1*$^{-/-}$ animals

To further elucidate the role of ERCC1 in WAT we scanned the transcriptome of 15-day-old wt and *Ercc1*$^{-/-}$ epididymal WAT (n=4). Two-way analysis of variance of Affymetrix mouse genome arrays revealed 2254 genes with significantly changed expression patterns between the *Ercc1*$^{-/-}$ and wt fat depots ($p \leq 0.05$, $\geq \pm 1.2$ fold change, Table S1). Using the set of 2254 genes, we identified those GO-classified biological processes with a significantly disproportionate number of responsive genes relative to those printed on microarrays (false detection rate ≤0.10). This approach revealed five biological processes involved in the response to DNA interstrand crosslinks (ICLs) and double-strand breaks (DSBs), pro-inflammatory signaling, nuclear receptor and growth factor signaling as well as a response to (oxidative) stress (Figure 3A). These transcriptional changes represent genuine changes in gene regulation as well as reflect a decrease in the fraction of adipocytes relative to stromal cells in *Ercc1*$^{-/-}$ WAT depots. *Ppar*$\gamma^{ldi/+}$ animals carry a targeted allele that confers conditional dominant lipodystrophy in mice (Kim et al., 2007). We, therefore, compared the gene expression profiles of 10-week old *Ppar*$\gamma^{ldi/+}$ and P15 *Ercc1*$^{-/-}$ gonadal fat pads. Despite the big difference in age between the two different animal models, we found 768 genes that changed significantly in WAT of both *Ppar*$\gamma^{ldi/+}$ and *Ercc1*$^{-/-}$ mice relative to their wt counterparts. This reflects 34% of the genes significantly altered in *Ercc1*$^{-/-}$ WAT compared to wt mice. Of these, 456 genes (20%) in *Ppar*$\gamma^{ldi/+}$ gonadal fat depots also shared

the same direction in expression (Figure 3B; Table S2). Interestingly, we find that PPARγ2, but not PPARγ1 protein and the mRNA levels are reduced in the 4-month old aP2-*Ercc1*$^{F/-}$ animals (Figure 3C–E and S3A). With the exception of the response to DNA ICLs/DSBs which was seen exclusively in *Ercc1*$^{-/-}$ mice, the set of 456 genes also found in *Pparγ*$^{ldi/+}$ fat depots was associated with the same over-represented biological themes identified in *Ercc1*$^{-/-}$ fat pads (Figure 3F). Quantitative (q) PCR and protein immunofluorescence analysis confirmed the validity of these results (Figure 4A–B). Taken together, these findings reveal that a gene expression signature of lipodystrophic fat is established early in *Ercc1*$^{-/-}$ progeroid mice.

A defect in *Ercc1*$^{-/-}$ WAT depots triggers accumulation of γ-H2AX, RAD51 and FANCI foci in aP2-*Ercc1*$^{F/-}$ gonadal fat pads

During NER, XPF-ERCC1 makes a single-strand nick near the lesion, which is critical for excision of the damage and thought to play an analogous role in DNA ICL repair (Niedernhofer et al., 2004). In line with the up-regulation of genes associated with the repair of DNA ICLs and DSBs in *Ercc1*$^{-/-}$ WAT depots, several genes associated with the repair of DNA ICLs and DSBs showed increased mRNA levels in 4-month old but the 1.5-month old aP2-*Ercc1*$^{F/-}$ WAT depots (Figure 4A). Phosphorylated histone H2A.X (γ-H2A.X)-containing foci accumulate at sites of DNA breaks (Fernandez-Capetillo et al., 2004). γ-H2A.X staining of aP2-*Ercc1*$^{F/-}$ adipocytes revealed a punctuate pattern of foci; γ-H2A.X gradually accumulated from 1–2 foci/nucleus in the 1.5-month old animals (~20% positive cells; data not shown) to approximately 3 or more foci/nucleus in the 4 month-old gonadal fat depots (~56% positive cells; Figure 4B and S3C). Similarly, RAD51, a protein involved in the repair of DSBs by homologous recombination (HR) (Elliott and Jasin, 2002) and FANCI involved in the repair of DNA inter-strand crosslinks (ICLs) (Sato et al., 2012) also formed foci that gradually increased from 1–2 foci/nucleus in the 1.5-month old mice to >10 foci/nucleus in 4-month old aP2-*Ercc1*$^{F/-}$ animals (Figure 4B and S3C). Similar to others, (Yang et al., 2011; Yang and Kastan, 2000), we found phosphorylated ATM to be predominantly cytoplasmic in adipocytes of 4-month old aP2-*Ercc1*$^{F/-}$ mice (Figure 4B and S3C). Staining with Caspase 3 revealed few, if any, apoptotic cells in 1.5- and 4-month old aP2-*Ercc1*$^{F/-}$ gonadal fat pads (data not shown). Instead, staining with TO-PRO-3 revealed a significant increase in necrotic cells (15.4%) in 4-month old aP2-*Ercc1*$^{F/-}$ WAT depots compared to age-matched controls or to 1.5-month old aP2-*Ercc1*$^{F/-}$ animals (Figure 4C and S3C). Damage-associated molecular pattern (DAMP) molecules are released by stressed cells undergoing necrosis that act as endogenous danger signals to promote and exacerbate defense responses, including inflammation (Miyake and Yamasaki, 2012). In 4-month old aP2-*Ercc1*$^{F/-}$ WAT, we detected the release of high-mobility group protein B1 (HMGB1), a central mediator of senescent phenotypes (Davalos et al., 2013) that is associated with DAMPs and is known to initiate and perpetuate immune responses in the noninfectious inflammatory response at sites of injury (Figure 4D) (Miyake and Yamasaki, 2012). HMGB1 protein levels were elevated in 4-month old aP2-*Ercc1*$^{F/-}$ WAT depots compared to those from age-matched wt mice or 1.5-month old mice (Figure 4E). Thus, tissue-specific ablation of *Ercc1* gene triggers the gradual accumulation of persistent cytotoxic DNA damage, which in turn causes necrotic cell death and the release of DAMPs on the surface of damaged adipocytes *in vivo*.

Persistent DNA damage triggers chronic inflammation in adipose tissue

The adipose tissue may host macrophages, which accumulate in so-called 'crown-like' structures (CLS) surrounding necrotic adipocytes (Murano et al., 2008). Unlike the 4-month old wt or the younger 1.5-month aP2-*Ercc1*$^{F/-}$ animals, confocal imaging of whole-mount 4-month old aP2-*Ercc1*$^{F/-}$ WAT revealed the presence of BrdU^{+} cells in CLS (Figure 5B and S4A) and infiltrating cells expressing macrophage antigens 1 (MAC1^{+}) and 3 (MAC3^{+}) that formed syncytia around dying adipocytes (Figure 5B and S4B). Both proteins are essential for leukocyte activation and MAC3 is a marker of differentiated macrophages (Khazen et al., 2005). Total white blood cell (WBC) counts and FACS analysis in 4-month old aP2-*Ercc1*$^{F/-}$ animals also revealed a significant increase in the number of WBCs and an increase of CD11b^{+} and CD11c^{+} stained cells in the stromal-vascular fraction, marking the presence of macrophages in these animals (Figure 5C and S4C–D). MAC1^{+} cells in 4-month old aP2-*Ercc1*$^{F/-}$ fat depots expressed iNOS, a potent inducer of chronic inflammation and a marker of activated macrophages (M1-type), CD45 a marker of leukocytes and two endothelial adhesion molecules ICAM-1 and VCAM, which are known to facilitate the accumulation of monocytes at sites of tissue injury (Figure 5D). ELISA assay on fat tissue revealed IL-6, TNF-α, and KC (murine homologue to IL-8) protein levels to be elevated in the 4-month old aP2-*Ercc1*$^{F/-}$ WAT depots compared to controls (Figure 5E). Similar data were found for TNF-α and KC protein levels in the 4-month old aP2-*Ercc1*$^{F/-}$ sera; IL-6 was undetectable (Figure S4F). Similarly, *Il6*, *Tnfa*, and *Kc* mRNA levels were increased in the adipose tissue of 4-month old aP2-*Ercc1*$^{F/-}$ animals compared to younger mice of the same genotype (Figure 5E; as indicated). As infiltrating macrophages could also express pro-inflammatory cytokines, we also analyzed the expression of *Il6*, *Tnfa*, and *Kc* mRNA levels in the stromal vascular and the adipocyte-rich fractions of 4-month old aP2-*Ercc1*$^{F/-}$ and aP2-*Ercc1*$^{F/+}$ WAT depots. Although, increased expression of pro-inflammatory cytokines was documented in both aP2-*Ercc1*$^{F/-}$ fractions compared to aP2-*Ercc1*$^{F/+}$ controls, the *Il6*, *Tnfa*, and *Kc* mRNA levels were substantially higher in the adipocyte-rich fraction compared to the stromal vascular fraction (Figure S4E). Similar data were found in *Ercc1*$^{\Delta/-}$ animals carrying a seven amino acid carboxyl terminal deletion in *Ercc1* gene (Weeda et al., 1997). Nine-week old *Ercc1*$^{\Delta/-}$ animals showed a substantial loss of WAT depots (n=9); we also find increased IL6, TNFα, and KC protein levels in the 9- and 20-week old *Ercc1*$^{\Delta/-}$ WAT depots as well as in the 20-week old *Ercc1*$^{\text{Delta;}/-}$ WAT depots at the mRNA level relative to control animals (n=4; Figure S4G–J). Together, our findings show that the formation of DNA damage foci correlates with the onset of pro-inflammatory signals in aP2-*Ercc1*$^{F/-}$ fat depots; the pro-inflammatory response is initiated by adipocytes rather than by infiltrating macrophages to necrotic adipocytes.

ICLs induce a pro-inflammatory response in adipocytes

Next, we used an *ex vivo* adipogenic assay to test whether DNA damage directly contributes to pro-inflammatory cytokine production in adipocytes. Naive primary wt and *Ercc1*$^{-/-}$ embryonic fibroblasts (MEFs) were exposed to an adipogenic stimulus for 13 days. This led to the *de novo* lipid accumulation marking the generation of differentiated, functional adipocytes expressing adipocyte-specific markers, including *Cebp4*, *Fabp4*, *Adiponectin* and *Adipsin* genes (Figure S5A). Unlike the wt adipocytes or undifferentiated *Ercc1*$^{-/-}$ MEFs,

Ercc1$^{-/-}$ adipocytes showed a dramatic accumulation of spontaneous γ-H2AX, pATM and FANCI, but not RAD51 foci (Figure 6A and S5B). In addition, *Ercc1*$^{-/-}$ adipocytes showed increased *Tnfa*, *Il6* and *Kc* mRNA levels compared to wt adipocytes when each was compared to undifferentiated controls, respectively (Figure 6B; **as indicated**). Thus, irreparable DNA lesions in otherwise unchallenged *Ercc1*$^{-/-}$ adipocytes trigger the production of pro-inflammatory factors. To further test this, we treated wt adipocytes with mitomycin C (MMC) for 2 hours, a potent inducer of DNA cross-links. This led to an increase in *Tnfa*, *Il6* and *Kc* mRNA levels (Figure 6B; **as indicated**); similar to our previous findings (Figure 6B), the increase in pro-inflammatory cytokine mRNA levels was substantially higher in MMC-treated adipocytes than MEFs relative to corresponding untreated controls. As the aP2 promoter selected in our work has been reported to be expressed also in macrophages (Mao et al., 2009), we tested whether *Ercc1* expression is compromised in macrophages at the origin of the phenotype observed in aP2-*Ercc1*$^{F/-}$ WAT depots. We find *Ercc1* levels in macrophages to be comparable at both the mRNA and the protein levels in the 2.5-month old aP2-*Ercc1*$^{F/-}$ compared to aP2-*Ercc1*$^{F/+}$ animals (Figure S1K–M). Taken together, our findings suggest that the transcription activation of pro-inflammatory cytokines is cell autonomous; it requires the presence of persistent DNA damage foci and is exacerbated in adipocytes compared to undifferentiated MEFs.

DNA damage signaling triggers histone changes associated with active transcription on promoters

To gain further mechanistic insight onto how the accumulation of persistent DNA damage foci leads to the transcriptional activation of *Tnfa*, *Il6* and *Kc* in *Ercc1*$^{-/-}$ adipocytes, we carried out a series of chromatin immunoprecipitation (ChIP) assays to examine the status of *Il6*, *Tnfa* and *Kc* promoters. Our analysis revealed substantial loss of repressive histone H3K9 and H3K27 trimethylation marks and a concomitant increase of activating acetylated histone H3K9 and H3K4 trimethylation marks in *Ercc1*$^{-/-}$ adipocytes compared to *Ercc1*$^{-/-}$ MEFs and in MMC-treated wt adipocytes compared to untreated controls (Figure 6C–D). Wt adipocytes also displayed an increase in activating histone marks compared to undifferentiated MEFs; however, unlike the *Ercc1*$^{-/-}$ adipocytes, repressive histone H3K9 and H3K27 trimethylation marks were maintained or increased in these cells (data not shown). Thus, a defect in DNA repair of spontaneous DNA damage or exposure of adipocytes to the genotoxin MMC triggers post-translational modifications of histones associated with active transcription in *Il6*, *Tnfa* and *Kc gene* promoters.

Persistent DNA damage signaling triggers the transcriptional de-repression of *Il6, Tnfα* and *Kc*

There is mounting evidence that at least some pro-inflammatory cytokines are in a poised yet repressed transcriptional state. Repression of active transcription is mediated by the recruitment of a co-repressor complex containing the nuclear receptor co-repressor (NCoR1) or the related silencing mediator of retinoic acid and thyroid hormone receptors (SMRT) on promoters (Perissi et al., 2010). PPARγ, whose protein and mRNA levels were substantially decreased in aP2-*Ercc1*$^{F/-}$ WAT depots, recruits SMRT and NCoR1 in the absence of ligand and these co-repressors are capable of down-regulating PPARγ-mediated transcriptional activity. In addition, NCoR1 and SMRT mediate active repression of their

respective target genes through the recruitment of additional co-repressor molecules, including the histone deacetylase HDAC3 (Perissi et al., 2010). Importantly, exposure of wt adipocytes to MMC led to the suppression of *Pparγ2* but not *Pparγ1* mRNA levels (Figure S3B). This and the up-regulation of *Il6, Tnfα* and *Kc* pro-inflammatory cytokine mRNA levels in *Ercc1*$^{-/-}$ fat depots prompted us to examine whether the co-repressor complex NCoR1-SMRT-HDAC3 is released from promoters in *Ercc1*$^{-/-}$ adipocytes or upon exposure of wt adipocytes to MMC. With the exception of NCoR1 for *Tnfα* promoter in *Ercc1*$^{-/-}$ adipocytes, we found substantially lower ChIP signals for the NCoR1, SMRT and HDAC3 on *Il6, Tnfα* and *Kc* promoters of *Ercc1*$^{-/-}$ adipocytes or MMC-treated wt adipocytes relative to corresponding controls (Figure 7A); intriguingly, we also find *Pparγ2*, but not *Pparγ1* mRNA levels to be substantially reduced in wt adipocytes exposed to MMC suggesting a functional link between DNA damage and the transcriptional downregulation of nuclear receptors in adipocytes (Figure S3B). Thus, defective DNA repair or exposure of wt adipocytes to a crosslinking agent triggers the transcriptional de-repression of pro-inflammatory cytokines.

The accumulation of ATM foci in the cytoplasm of 4-month old aP2-*Ercc1*$^{F/-}$ adipocytes prompted us to test whether ATM is required for the DNA damage-driven transcriptional de-repression of *Il6, Tnfα* and *Kc* in adipocytes. Inactivation of ATM by exposing MMC-treated adipocytes to KU-55933 inhibitor known to ablate DNA damage-induced phosphorylation of ATM substrates (Ding et al., 2006) significantly abrogated the release of repressor complexes from promoters and abolished the transcriptional induction of *Il6, Tnfα* and *Kc* mRNA levels in these cells (Figure 7B). We also exposed MMC-treated adipocytes to ATR/CDK Inhibitor i.e. NU6027 known to inhibit ATR kinase without interfering with irradiation-induced autophosphorylation of DNA-PK or ATM. Inactivation of ATR led to similar results with those seen upon ATM inactivation, albeit to a smaller magnitude (Figure 7B). Thus, while ATR may contribute to the transcriptional de-repression of promoters, ATM is essential in linking the nuclear DDR signaling to the transcriptional activation of pro-inflammatory cytokines in aP2-*Ercc1*$^{F/-}$ WAT depots. Similarly, activation of the anti-inflammatory PPARγ by exposing MMC-treated adipocytes to Rosiglitazone, a PPARγ agonist, significantly abrogated the transcriptional induction of *Il6, Tnfα* and *Kc* mRNA levels (Figure 7B). To test whether ATM and PPARγ play similar roles in *Ercc1*$^{-/-}$ adipocytes, we inhibited ATM or activated PPARγ in *Ercc1*$^{-/-}$ adipocytes; importantly, treatment of *Ercc1*$^{-/-}$ adipocytes with KU-55933 inhibitor or Rosiglitazone significantly abrogated the transcriptional induction of *Il6, Tnfα* and *Kc* mRNA levels compared to untreated controls (Figure 7C), a finding that was also confirmed in ATMi-treated adipocyte culture media for TNF-α protein levels (Figure S5D). Finally, we find that *Ercc1* mRNA levels are significantly decreased whereas *Il6, Tnfa* and *Kc* mRNA levels are significantly increased in 110-week old compared to 6-week old wt fat depots (Figure S5C). Thus, our findings provide a model by which persistent DNA damage in aP2-*Ercc1*$^{-/-}$ fat depots *in vivo* and in adipocytes *ex vivo* trigger the induction of pro-inflammatory cytokines by promoting transcriptionally active histone marks and the dissociation of nuclear receptor co-repressor complexes from promoters (Figure 7C).

Discussion

How DNA damage triggers the onset of tissue-specific pathology in NER patients and accompanying mouse models remains an intriguing question arguing for tissue-specific responses against deleterious threats. Besides cachectic dwarfism, *Ercc1*$^{-/-}$ mice show several progeroid features, including the noticeable loss of adipose tissue depots. To distinguish between causative and indirect mechanisms of fat depletion in the ERCC1-deficient mice, we focused our studies on fat-specific aP2-*Ercc1*$^{F/-}$ animals. Because aP2 gene expression does not peak until the adipocyte is mature (Tang et al., 2008), ERCC1 is deleted at a later stage in the aP2-*Ercc1*$^{F/-}$ animals. This allows us to gain insights into the effect of time-dependent accumulation of DNA damage on adult fat depots. Importantly, aP2-*Ercc1*$^{F/-}$ mice are born with Mendelian frequency, grow normally, are fertile and show no visible pathological signs until adulthood. Beginning at 2.5-months, however, aP2-*Ercc1*$^{F/-}$ mice exhibit marked signs of lipodystrophy including a considerable decrease in adipocyte size, tissue necrosis and fibrosis in injured sites as well as metabolic abnormalities that are associated with insulin resistance and diabetes mellitus type II. Although fat depletion and obesity are opposites in terms of fat mass, both conditions are accompanied by similar metabolic abnormalities, inflammation and macrophage infiltration into adipose tissue depots; the latter are, however, different in terms of abundance, activation state and gene expression (Herrero et al., 2010).

Importantly, aP2-*Ercc1*$^{F/-}$ fat depots showed hallmarks of persistent DDR; ATM foci appeared predominantly in the cytoplasm supporting recent observations that link cytoplasmic ATM with downstream cytokine signaling (Hinz et al., 2010). Persistent DDR foci in aP2-*Ercc1*$^{F/-}$ fat depots appeared together with the up-regulation of pro-inflammatory factors, the infiltration of activated macrophages in CLS as well as the release of DAMPs, such as HMGB1, that can trigger cytokine release further propagating the inflammatory response in damaged fat depots (Sims et al., 2010). Thus, persistent DDR signaling closely correlates with inflammatory cytokine production at damaged aP2-*Ercc1*$^{F/-}$ fat depots.

The presence of FANCI foci without RAD51 foci in *Ercc1*$^{-/-}$ adipocytes argues for the presence of irreparable DNA ICLs in these cells; however, as RAD51 is also needed for ICL repair, our findings suggest that ICL damage signaling is activated, but in the absence of incision by ERCC1-XPF, DNA repair cannot take place, hence the absence of HR foci. The lack of DDR foci formation in unchallenged *Ercc1*$^{-/-}$ MEFs (as compared to *Ercc1*$^{-/-}$ adipocytes) suggests that certain types of cells i.e. adipocytes experience high levels of genotoxic stress. Lipid peroxide is an endogenous source of crosslinking agents (Niedernhofer et al., 2003). In WAT, where lipids are most abundant, inflammation and consequent lipid peroxidation could trigger the formation of more DNA ICLs. This and the inherent propensity of adipocytes to secrete pro-inflammatory signals upon metabolic stress (Tchkonia et al., 2010) could establish self-perpetuating pro-inflammatory cycles leading to systemic metabolic dysfunction. Unlike the *Ercc1*$^{-/-}$ WAT depots, *Ercc1*$^{-/-}$ cells did not show a cytoplasmic localization of ATM likely reflecting lineage-specific differences between adipocytes and MEFs exposed to adipogenic differentiation media (Li et al., 2009).

In our work, abrogation of ERCC1 in adipocytes or exposure of wt adipocytes to MMC crosslinking agent led to the transcriptional activation of pro-inflammatory cytokines *in vitro*. DNA damage was sufficient to trigger the expression of pro-inflammatory cytokines whether or not cells were competent to proliferate. Previous studies suggest that human cells induced to senesce by genotoxic stress secrete several pro-inflammatory factors (Coppe et al., 2008). However, cells induced to senesce by p16INK4a expression, but in the absence of DNA damage, did not initiate a cytokine response (Rodier et al., 2009) further supporting our observations that DDR can independently trigger a pro-inflammatory response in aP2-*Ercc1*$^{F/-}$ fat depots.

Whereas genes that mediate inflammatory responses must be kept tightly repressed under normal conditions, they must also be rapidly induced in the setting of tissue injury. PPARγ is a nuclear hormone receptor that has potent anti-inflammatory roles (Straus and Glass, 2007). The P15 *Ercc1*$^{-/-}$ WAT depots showed decreased PPARγ2 mRNA and protein levels and a considerable overlap in gene expression changes with 10-week old *Pparγ*$^{ldi/+}$ adult animals. As PPARγ modulates responses by forming protein complexes with co-activators or co-repressors on promoters (Guan et al., 2005), we asked whether a similar mechanism could initiate the transition of pro-inflammatory genes from a repressed to an actively transcribed state in adipocytes. Abrogation of ERCC1 in adipocytes or exposure of wt adipocytes to MMC triggers histone post-translational modifications that associate with active transcription of pro-inflammatory factors in adipocytes. Subsequent studies in *Ercc1*$^{-/-}$ and MMC-treated wt adipocytes revealed the dissociation of co-repressors NCoR1, SMRT and HDAC3 from promoters closely matching the increase of *IL-6*, *TNFα* and *KC* mRNA levels in these cells. Importantly, ATM, and to a lesser extent also ATR, inactivation abolished the DNA damage-driven release of co-repressor complexes from promoters and the induction of pro-inflammatory cytokine expression in adipocytes. Thus, the transcriptional derepression of pro-inflammatory genes in adipocytes requires DDR signaling with active ATM playing a prominent role in mediating the pro-inflammatory response to persistent genotoxic stress in fat depots.

It has been challenging to delineate how different cell populations respond to DNA damage *in vivo*, and the mechanism by which DNA damage drives tissue-specific pathology in NER progeroid syndromes. Here, we provide evidence for a functional link between persistent DNA damage and loss of fat depots, a feature of accelerated and natural aging. Using mice carrying an adipose tissue-specific defect in ERCC1-XPF DNA repair endonuclease, we provide *in vivo* evidence that the gradual accumulation of irreparable DNA lesions in *Ercc1*$^{-/-}$ adipocytes triggers a chronic auto-inflammatory response leading to adipose tissue degeneration. In the short-term, this response would allow damaged cells to communicate their compromised state to the microenvironment; in the long-term, however, it leads to age-related degeneration and loss of fat depots.

Experimental procedures

Animal studies

Ercc1^{F} mice containing a floxed allele of the *Ercc1* gene (Verhagen-Oldenampsen et al., 2012) and Rosa26-YFP$^{st/st}$ mice were crossed with Fabp4 (aP2)-*Cre* transgenic mice to

obtain inactivation of the *Ercc1* gene or expression of YFP in adipocytes, respectively. For insulin and glucose tolerance tests, mice were injected intraperitoneally with 0.75 Units/kg of body weight insulin (Humulin, Ely Lili) or with 1 g/kg of body weight 35% dextrose solution, respectively. For BrdU incorporation studies, mice were injected intraperitoneally with 30 mg/kg of body weight BrdU (Sigma) in 1x PBS and sacrificed 48 hours later. An independent Animal Ethical Committee at the IMBB-FORTH approved the animal studies. Detailed information on experimental procedures is described in the supplemental section.

Scanning electron microscopy

For scanning electron microscopy (SEM), fresh adipose tissue was cut into small blocks, fixed and specimens were coated in gold, mounted on aluminum stubs and examined with a JEOL JSM6390 LV scanning electron microscope (Peabody, MA) using an accelerating voltage of 15 kV.

Histology

For lipids staining, OCT-embedded tissues were cryosectioned, fixed in 10% formalin, stained with Oil Red O and counterstained with Harris's Haematoxylin. For insulin staining, paraffin-embedded pancreata were sectioned, de-paraffinized, boiled in 10 mM Sodium Citrate buffer, stained with anti-insulin antibody (Cell Signaling Technology) and visualized with DAB chromogen (Sigma).

Microarrays and qPCR assays

Microarrays, qPCR, and qPCR data analysis were performed as previously described (Kamileri et al., 2012b). Primer sequences for the genes tested by qPCR are available upon request. Microarray data can be retrieved from Arrayexpress (http://www.ebi.ac.uk/arrayexpress/); accession number: E-MEXP-3930.

Immunostaining, western blots, ChIP assays and antibodies

Immunofluorescence experiments were performed as previously described (Garinis et al., 2005; Nishimura et al., 2008) and visualized with a Leica TCS SP2 SE confocal microscope. For ChIP assays, cells were crosslinked with 1% formaldehyde, chromatin was sonicated using an Ultrasonic homogenizer and samples were immunoprecipitated with antibodies and protein G Sepharose beads (Millipore, USA). Purified DNA fragments were analyzed by qPCR using primers targeting different regions of *IL6, TNF and KC* genes. Detailed information is described in the supplemental section.

Inflammatory Cell Counts – FACS analysis

Epididymal adipose tissue fragments were incubated in 1x HBS buffer supplemented with 2 mg/ml Collagenase (Sigma) for 1 hour at 37 C. The Stromal Vascular fraction was collected by centrifugation and cells were filtered to obtain single cell suspensions. White blood cell counts per mouse were estimated using Kimura stain (Kimura et al., 1973). To estimate adipose tissue inflammatory cells by FACS analysis, cells were stained with FITC-CD11b (BD Biosciences) or FITC-CD11c antibodies (BioLegend). Flow cytometry events were

acquired with a MoFlo Legacy Cell Sorter (Beckman Coulter) and analyzed using the Summit Software.

Cell culture and *ex vivo* adipogenesis assays

Two-day post confluent primary MEFs were induced for adipocyte differentiation with standard medium supplemented with an adipogenic cocktail. Adipocytes and undifferentiated MEFs were treated with 10 μg/μl mitomycin C (AppliChem) for 2 hours in serum-free DMEM and were recovered after 6 hours in standard medium. For ATM or ATR kinase inhibitor assays, cells were treated for 1 hour with 10 μM inhibitor (Millipore), followed by the addition of MMC. *Ercc1*$^{-/-}$ MEFs were treated with ATMi for 48 hours or with 0.5 μ Rosiglitazone (SantaCruz Biotechnology) throughout differentiation.

Data analysis

For microarrays, two-tail, pair-wise analysis or a two-way analysis of variance was used to extract the statistically significant gene expression data by means of the IBM SPSS Statistics 19 (IBM, NY, USA), Spotfire (Tibco, CA, USA), Partek (Partek INCoR1porated, MO, USA) and R-statistical package (www.r-project.org/). Significant overrepresentation of pathways and gene networks was determined by DAVID (http://david.abcc.ncifcrf.gov/summary.jsp; through BBID, BIOCARTA and KEGG annotations) as well as by means of the ingenuity pathway analysis software (www.ingenuity.com). Detailed information is described in the supplemental section.

Supplementary Material

Refer to Web version on PubMed Central for supplementary material.

Acknowledgments

The NSRF-ESPA 2007-2013 “Heracleitus II”, the “Cooperation” No: EDGE 901-13/11/2009, the THALIS (ESPA 2007-2013) “GenAge” and “miREG”, the ARISTEIA “TagNER” and the ELKE 901-13/11/2009 (NSRF 2007-2013) and the FP7 Marie Curie ITN “aDDRess, “CodeAge” and “Marriage” funds supported this work. I.K. is supported by the Maria-Michail Manassakis fellowship. A.R.R. and L.J.N. were supported by NIH (ES016114). G.A.G is supported by the EMBO Young Investigator program. None of the authors of this work has a financial interest related to this work.

References

Coppe JP, Patil CK, Rodier F, Sun Y, Munoz DP, Goldstein J, Nelson PS, Desprez PY, Campisi J. Senescence-associated secretory phenotypes reveal cell-nonautonomous functions of oncogenic RAS and the p53 tumor suppressor. PLoS biology. 2008; 6:2853–2868. [PubMed: 19053174]

Davalos AR, Kawahara M, Malhotra GK, Schaum N, Huang J, Ved U, Beausejour CM, Coppe JP, Rodier F, Campisi J. p53-dependent release of Alarmin HMGB1 is a central mediator of senescent phenotypes. The Journal of cell biology. 2013

DiGiovanna JJ, Kraemer KH. Shining a light on xeroderma pigmentosum. The Journal of investigative dermatology. 2012; 132:785–796. [PubMed: 22217736]

Ding J, Miao ZH, Meng LH, Geng MY. Emerging cancer therapeutic opportunities target DNA-repair systems. Trends in pharmacological sciences. 2006; 27:338–344. [PubMed: 16697054]

Elliott B, Jasin M. Double-strand breaks and translocations in cancer. Cell Mol Life Sci. 2002; 59:373–385. [PubMed: 11915950]

Fernandez-Capetillo O, Lee A, Nussenzweig M, Nussenzweig A. H2AX: the histone guardian of the genome. DNA repair. 2004; 3:959–967. [PubMed: 15279782]

Garinis GA, Mitchell JR, Moorhouse MJ, Hanada K, de Waard H, Vandeputte D, Jans J, Brand K, Smid M, van der Spek PJ, et al. Transcriptome analysis reveals cyclobutane pyrimidine dimers as a major source of UV-induced DNA breaks. The EMBO journal. 2005; 24:3952–3962. [PubMed: 16252008]

Garinis GA, van der Horst GT, Vijg J, Hoeijmakers JH. DNA damage and ageing: new-age ideas for an age-old problem. Nature cell biology. 2008; 10:1241–1247.

Guan HP, Ishizuka T, Chui PC, Lehrke M, Lazar MA. Corepressors selectively control the transcriptional activity of PPARgamma in adipocytes. Genes & development. 2005; 19:453–461. [PubMed: 15681609]

Hanawalt PC. Subpathways of nucleotide excision repair and their regulation. Oncogene. 2002; 21:8949–8956. [PubMed: 12483511]

Hegele RA, Joy TR, Al-Attar SA, Rutt BK. Thematic review series: Adipocyte Biology. Lipodystrophies: windows on adipose biology and metabolism. Journal of lipid research. 2007; 48:1433–1444. [PubMed: 17374881]

Herrero L, Shapiro H, Nayer A, Lee J, Shoelson SE. Inflammation and adipose tissue macrophages in lipodystrophic mice. Proceedings of the National Academy of Sciences of the United States of America. 2010; 107:240–245. [PubMed: 20007767]

Hinz M, Stilmann M, Arslan SC, Khanna KK, Dittmar G, Scheidereit C. A cytoplasmic ATM-TRAF6-cIAP1 module links nuclear DNA damage signaling to ubiquitin-mediated NF-kappaB activation. Molecular cell. 2010; 40:63–74. [PubMed: 20932475]

Jones JR, Barrick C, Kim KA, Lindner J, Blondeau B, Fujimoto Y, Shiota M, Kesterson RA, Kahn BB, Magnuson MA. Deletion of PPARgamma in adipose tissues of mice protects against high fat diet-induced obesity and insulin resistance. Proc Natl Acad Sci U S A. 2005; 102:6207–6212. [PubMed: 15833818]

Kadowaki T, Yamauchi T, Kubota N, Hara K, Ueki K, Tobe K. Adiponectin and adiponectin receptors in insulin resistance, diabetes, and the metabolic syndrome. The Journal of clinical investigation. 2006; 116:1784–1792. [PubMed: 16823476]

Kamileri I, Karakasilioti I, Garinis GA. Nucleotide excision repair: new tricks with old bricks. Trends in genetics: TIG. 2012a

Kamileri I, Karakasilioti I, Sideri A, Kosteas T, Tatarakis A, Talianidis I, Garinis GA. Defective transcription initiation causes postnatal growth failure in a mouse model of nucleotide excision repair (NER) progeria. Proceedings of the National Academy of Sciences of the United States of America. 2012b; 109:2995–3000. [PubMed: 22323595]

Khazen W, M'Bika JP, Tomkiewicz C, Benelli C, Chany C, Achour A, Forest C. Expression of macrophage-selective markers in human and rodent adipocytes. FEBS letters. 2005; 579:5631–5634. [PubMed: 16213494]

Kim S, Huang LW, Snow KJ, Ablamunits V, Hasham MG, Young TH, Paulk AC, Richardson JE, Affourtit JP, Shalom-Barak T, et al. A mouse model of conditional lipodystrophy. Proceedings of the National Academy of Sciences of the United States of America. 2007; 104:16627–16632. [PubMed: 17921248]

Kimura I, Moritani Y, Tanizaki Y. Basophils in bronchial asthma with reference to reagin-type allergy. Clin Allergy. 1973; 3:195–202. [PubMed: 4131253]

Li J, Han YR, Plummer MR, Herrup K. Cytoplasmic ATM in neurons modulates synaptic function. Current biology: CB. 2009; 19:2091–2096. [PubMed: 19962314]

Mao J, Yang T, Gu Z, Heird WC, Finegold MJ, Lee B, Wakil SJ. aP2-Cre-mediated inactivation of acetyl-CoA carboxylase 1 causes growth retardation and reduced lipid accumulation in adipose tissues. Proceedings of the National Academy of Sciences of the United States of America. 2009; 106:17576–17581. [PubMed: 19805143]

Miyake Y, Yamasaki S. Sensing necrotic cells. Advances in experimental medicine and biology. 2012; 738:144–152. [PubMed: 22399378]

Murano I, Barbatelli G, Parisani V, Latini C, Muzzonigro G, Castellucci M, Cinti S. Dead adipocytes, detected as crown-like structures, are prevalent in visceral fat depots of genetically obese mice. Journal of lipid research. 2008; 49:1562–1568. [PubMed: 18390487]

Niedernhofer LJ, Daniels JS, Rouzer CA, Greene RE, Marnett LJ. Malondialdehyde, a product of lipid peroxidation, is mutagenic in human cells. The Journal of biological chemistry. 2003; 278:31426–31433. [PubMed: 12775726]

Niedernhofer LJ, Garinis GA, Raams A, Lalai AS, Robinson AR, Appeldoorn E, Odijk H, Oostendorp R, Ahmad A, van Leeuwen W, et al. A new progeroid syndrome reveals that genotoxic stress suppresses the somatotroph axis. Nature. 2006; 444:1038–1043. [PubMed: 17183314]

Niedernhofer LJ, Odijk H, Budzowska M, van Drunen E, Maas A, Theil AF, de Wit J, Jaspers NG, Beverloo HB, Hoeijmakers JH, et al. The structure-specific endonuclease Ercc1-Xpf is required to resolve DNA interstrand cross-link-induced double-strand breaks. Molecular and cellular biology. 2004; 24:5776–5787. [PubMed: 15199134]

Nishimura S, Manabe I, Nagasaki M, Seo K, Yamashita H, Hosoya Y, Ohsugi M, Tobe K, Kadowaki T, Nagai R, et al. In vivo imaging in mice reveals local cell dynamics and inflammation in obese adipose tissue. The Journal of clinical investigation. 2008; 118:710–721. [PubMed: 18202748]

Perissi V, Jepsen K, Glass CK, Rosenfeld MG. Deconstructing repression: evolving models of co-repressor action. Nature reviews Genetics. 2010; 11:109–123.

Rodier F, Coppe JP, Patil CK, Hoeijmakers WA, Munoz DP, Raza SR, Freund A, Campeau E, Davalos AR, Campisi J. Persistent DNA damage signalling triggers senescence-associated inflammatory cytokine secretion. Nature cell biology. 2009; 11:973–979.

Satir P, Pedersen LB, Christensen ST. The primary cilium at a glance. J Cell Sci. 2010; 123:499–503. [PubMed: 20144997]

Sato K, Ishiai M, Toda K, Furukoshi S, Osakabe A, Tachiwana H, Takizawa Y, Kagawa W, Kitao H, Dohmae N, et al. Histone chaperone activity of Fanconi anemia proteins, FANCD2 and FANCI, is required for DNA crosslink repair. The EMBO journal. 2012; 31:3524–3536. [PubMed: 22828868]

Schumacher B, Hoeijmakers JH, Garinis GA. Sealing the gap between nuclear DNA damage and longevity. Molecular and cellular endocrinology. 2009; 299:112–117. [PubMed: 19027821]

Selfridge J, Hsia KT, Redhead NJ, Melton DW. Correction of liver dysfunction in DNA repair-deficient mice with an ERCC1 transgene. Nucleic acids research. 2001; 29:4541–4550. [PubMed: 11713303]

Sepe A, Tchkonia T, Thomou T, Zamboni M, Kirkland JL. Aging and regional differences in fat cell progenitors - a mini-review. Gerontology. 2011; 57:66–75. [PubMed: 20110661]

Sims GP, Rowe DC, Rietdijk ST, Herbst R, Coyle AJ. HMGB1 and RAGE in inflammation and cancer. Annual review of immunology. 2010; 28:367–388.

Straus DS, Glass CK. Anti-inflammatory actions of PPAR ligands: new insights on cellular and molecular mechanisms. Trends in immunology. 2007; 28:551–558. [PubMed: 17981503]

Tang W, Zeve D, Suh JM, Bosnakovski D, Kyba M, Hammer RE, Tallquist MD, Graff JM. White fat progenitor cells reside in the adipose vasculature. Science. 2008; 322:583–586. [PubMed: 18801968]

Tchkonia T, Morbeck DE, Von Zglinicki T, Van Deursen J, Lustgarten J, Scrable H, Khosla S, Jensen MD, Kirkland JL. Fat tissue, aging, and cellular senescence. Aging cell. 2010; 9:667–684. [PubMed: 20701600]

Verhagen-Oldenampsen JH, Haanstra JR, van Strien PM, Valkhof M, Touw IP, von Lindern M. Loss of ercc1 results in a time- and dose-dependent reduction of proliferating early hematopoietic progenitors. Anemia. 2012; 2012:783068. [PubMed: 22701168]

Weeda G, Donker I, de Wit J, Morreau H, Janssens R, Vissers CJ, Nigg A, van Steeg H, Bootsma D, Hoeijmakers JH. Disruption of mouse ERCC1 results in a novel repair syndrome with growth failure, nuclear abnormalities and senescence. Current biology: CB. 1997; 7:427–439. [PubMed: 9197240]

Yang DQ, Halaby MJ, Li Y, Hibma JC, Burn P. Cytoplasmic ATM protein kinase: an emerging therapeutic target for diabetes, cancer and neuronal degeneration. Drug discovery today. 2011; 16:332–338. [PubMed: 21315178]

Yang DQ, Kastan MB. Participation of ATM in insulin signalling through phosphorylation of eIF-4E-binding protein 1. Nature cell biology. 2000; 2:893–898.

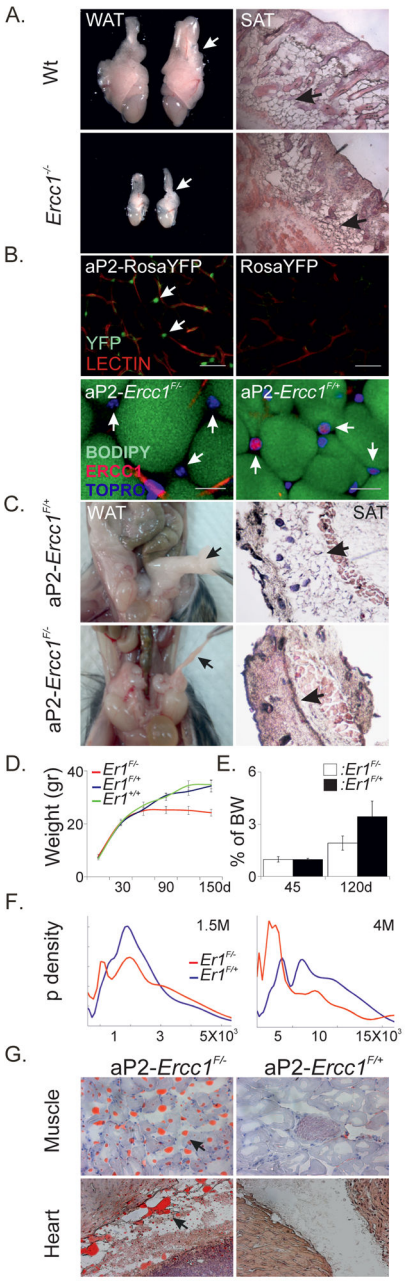

Figure 1. Loss of fat depots in *Ercc1*$^{-/-}$ and aP2-*Ercc1*$^{F/-}$ animals

(A). Photograph of 15-day old wt and *Ercc1*$^{-/-}$ epididymal white adipose tissue (embedded arrowheads; WAT) and subcutaneous (embedded arrowheads; SAT) depots. **(B).** aP2-*Cre* -driven Rosa-YFP expression in adipocytes (upper panel) and ERCC1 protein staining indicating cell type-specific ablation of ERCC1 in aP2-*Ercc1*$^{F/-}$ adipocytes (lower panel) indicated by the respective arrows. **(C).** Photograph of 4-month old aP2-*Ercc1*$^{F/+}$ and aP2-*Ercc1*$^{F/-}$ WAT and SAT depots indicated by the respective arrows. **(D).** Weight of aP2-*Ercc1*$^{F/-}$ (*Er1*$^{F/-}$), aP2-*Ercc1*$^{F/+}$ (*Er1*$^{F/+}$) and wt (*Er*$^{+/+}$) animals at the indicated timepoints and **(E).** Weight of WAT depots shown as % of body weight (BW). **(F).** Size distribution of adipocytes derived from 1.5- and 4-month old aP2-*Ercc1*$^{F/-}$ (*Er1*$^{F/-}$) and aP2-*Ercc1*$^{F/+}$

($Er1^{F/+}$) animals. **(G).** Oil Red O staining indicating the accumulation of triglycerides in muscle and heart tissues derived from 4-month old aP2-$Ercc1^{F/-}$ as compared to aP2-$Ercc1^{F/+}$ animals (20x magnification). Scale bars: 50 μm (RosaYFP), 20 μm (ERCC1), error bars indicate S.E.M. (n ≥ 3). See also Figure S1.

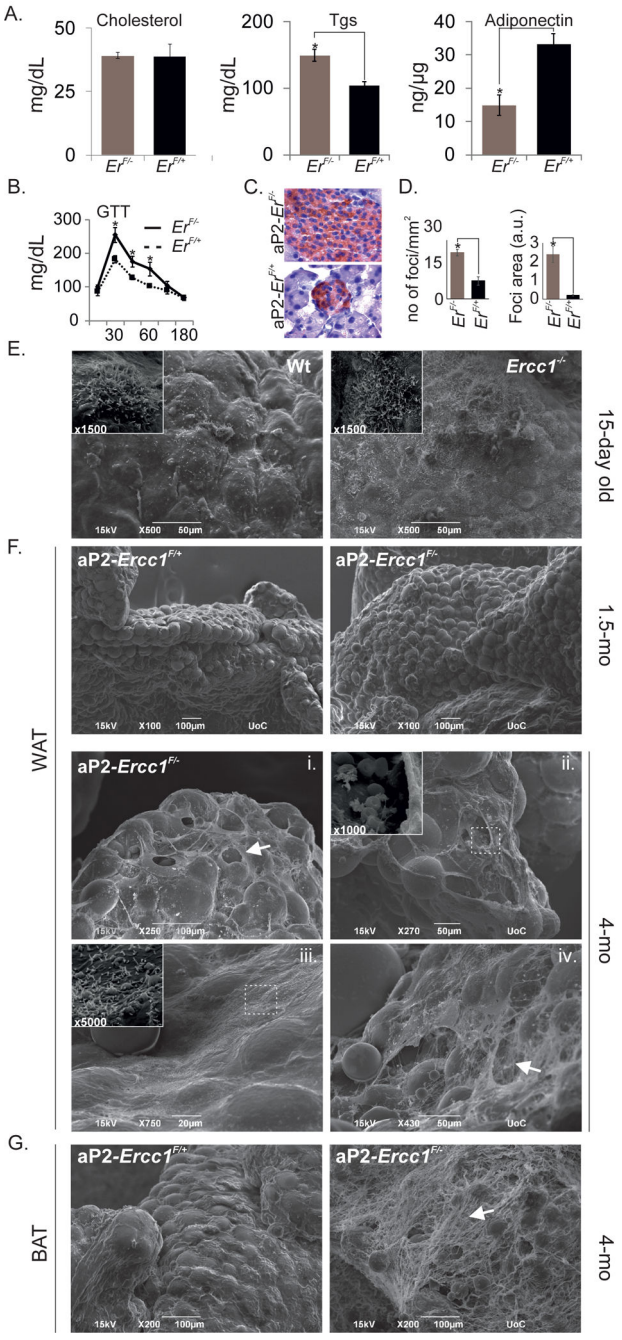

Figure 2. Progressive lipodystrophy in aP2-*Ercc1*$^{F/-}$ mice

(A). Serum cholesterol, triglycerides (TGs) and white adipose tissue adiponectin levels of 4-month old aP2-*Ercc1*$^{F/-}$ (*Er1*$^{F/-}$) and aP2-*Ercc1*$^{F/+}$ (*Er1*$^{F/+}$) animals (n=4; as indicated). **(B).** Glucose tolerance test (GTT) in 4-month old aP2-*Ercc1*$^{F/-}$ (*Er1*$^{F/-}$) and aP2-*Ercc1*$^{F/+}$ (*Er1*$^{F/+}$) animals (n=4). **(C).** Immunohistochemical analysis of 4-month old aP2-*Ercc1*$^{F/-}$ (*Er1*$^{F/-}$) and aP2-*Ercc1*$^{F/+}$ (*Er1*$^{F/+}$) pancreata showing staining of β cells, using insulin antibody. **(D).** Estimates of number and area of pancreatic islets stained for insulin in the 4-month old aP2-*Ercc1*$^{F/-}$ (*Er1*$^{F/-}$) and aP2-*Ercc1*$^{F/+}$ (*Er1*$^{F/+}$) animals (n=4; as indicated).

(E). Representative scanning electron micrographs of 15-day old wt and *Ercc1*$^{-/-}$ perigonadal white adipose tissue (WAT) depots. Insert: higher magnification indicating ciliae in both tissues. **(F).** Representative scanning electron micrographs of 1.5-month old aP2-*Ercc1*$^{F/+}$ and aP2-*Ercc1*$^{F/-}$ WAT depots (upper panel) and 4-month old aP2-*Ercc1*$^{F/-}$ WAT depots (lower panels). Note the i) basement membrane rupture, ii) adipocyte depletion (index: presence of red blood cells indicating capillary destruction), iii) re-appearance of ciliae and iv) extensive fibrosis. **(G).** Representative scanning electron micrographs of 4-month old aP2-*Ercc1*$^{F/+}$ and aP2-*Ercc1*$^{F/-}$ brown adipose tissue (BAT) depots. Note the extensive fibrosis in aP2-*Ercc1*$^{F/-}$ BAT depots. P-value: *≤0.05; a.u.: arbitrary units; error bars indicate S.E.M. (n≥3). See also Figure S2.

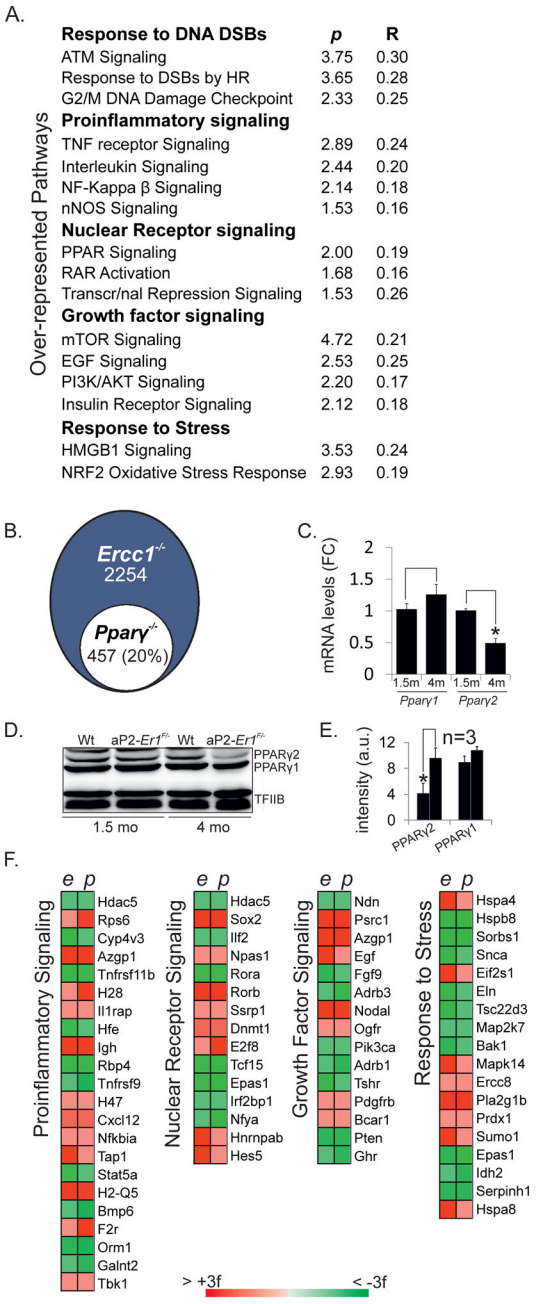

Figure 3. Transcriptome analysis of perigonadal WAT depots in *Ercc1*$^{-/-}$ mice

(A). Over-represented biological processes in *Ercc1*$^{-/-}$ perigonadal white adipose tissue (WAT) depots compared to age-matched wt mice; *p:* -log of p-value which is calculated by Fisher's exact test right-tailed, R: ratio of number of genes in the indicated pathway divided by the total number of genes that make up that pathway. **(B).** Venn's logic representing genes with shared expression changes between *Ercc1*$^{-/-}$ and *Pparγ*$^{ldi/-}$ WAT depots. **(C).** mRNA levels of *Pparγ1* and *2* in 1.5- and 4-month old aP2-*Ercc1*$^{F/-}$ WAT depots, compared to age-matched aP2-*Ercc1*$^{F/+}$controls, which were set to 1. The graphs represent the average from 4 mice +/− SEM. Asterisk indicates significance p≤0.05 using a two-tailed

Student's t-test. **(D).** Western blot and **(E).** Quantification of protein levels of PPARγ1 and 2 in 1.5- and 4-month old aP2-*Ercc1*$^{F/+}$ and aP2-*Ercc1*$^{F/-}$ WAT depots. **(F).** Heat-map representation of significant gene expression changes between *Ercc1*$^{-/-}$(*e*) and *Pparγ*$^{Jdi/-}$ (*p*) WAT depots. Data represent the average of 3 mice +/− SEM. Asterisk indicates significance $p \leq 0.05$ using a two tailed Student's t-test. See also Figure S3, Table S1 and Table S2.

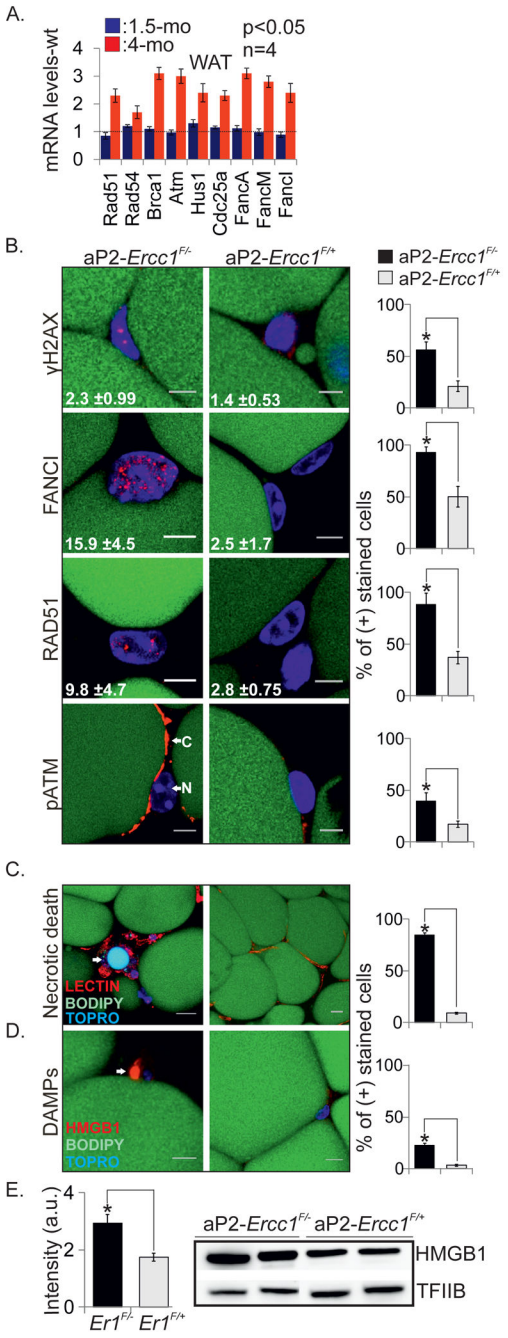

Figure 4. The *Ercc1* defect triggers a response to DNA ICLs and DSBs in aP2-*Ercc1*$^{F/-}$ fat depots

(A). Quantitative (q) PCR mRNA levels of genes associated with a response to DNA ICLs and DSBs in 1.5- and 4-month old aP2-*Ercc1*$^{F/-}$ perigonadal white adipose tissue (WAT) depots. Black dotted line: wt mRNA levels. **(B)**. Immunofluorescence detection of γ-H2AX, FANCI, RAD51 and pATM foci in aP2-*Ercc1*$^{F/-}$ and aP2-*Ercc1*$^{F/+}$ WAT depots. Note the cytoplasmic localization of pATM foci. Graphs show the % of positively stained cells ± st.dev (n=3). Lower number depicts the average number of foci per cell ± st.dev. **(C).** Immunofluorescence detection of TO-PRO 3 in non-permeabilized cells indicating necrotic

cell death and **(D).** HMGB1 release from chromatin in 4-month old aP2-*Ercc1*$^{F/-}$ and aP2-*Ercc1*$^{F/+}$ WAT depots. Graphs show the % of positively stained cells ± st.dev. **(E).** Western blot levels of HMGB1 in 4-month old aP2-*Ercc1*$^{F/-}$ and aP2-*Ercc1*$^{F/+}$ WAT depots. N: nucleus, C: cytoplasm. Error bars indicate S.E.M. among replicates of 3 or more animals, scale bars: b=5 μm, c=50 μm, d=20 μm. P-value: *≤0.05; a.u.: arbitrary units. See also Figure S3.

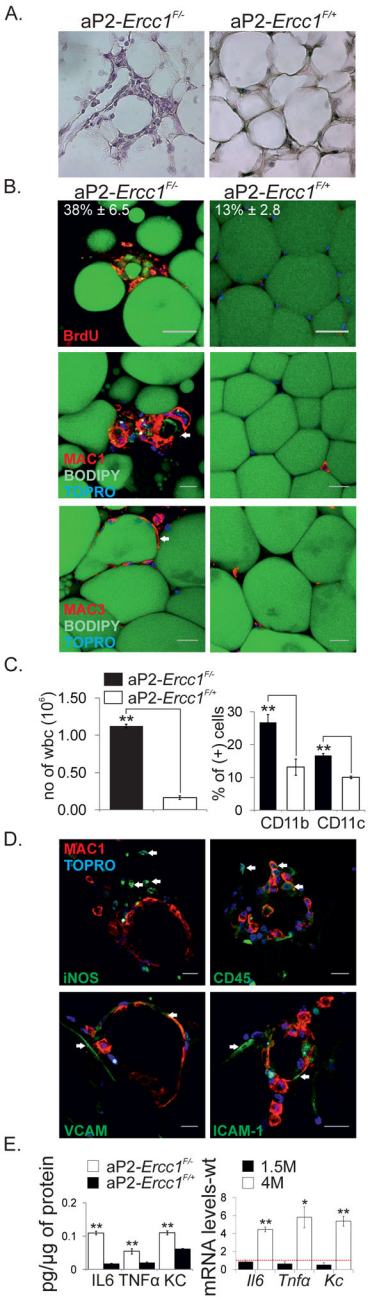

Figure 5. Tissue-specific ablation of ERCC1 triggers an inflammatory response in aP2-*Ercc1*$^{F/-}$ adipose tissue depots

(A). Hematoxylin-Eosin staining of 4-month old aP2-*Ercc1*$^{F/-}$ perigonadal white adipose tissue (WAT) depots indicating the formation of crown-like structures (CLS) compared to aP2-*Ercc1*$^{F/+}$ controls. **(B).** Confocal imaging of whole-mount aP2-*Ercc1*$^{F/-}$ WAT indicating the presence of BrdU^{+} cells in CLS and infiltrating MAC1^{+} and MAC3^{+} macrophages forming syncytia around dying adipocytes as compared to aP2-*Ercc1*$^{F/+}$ controls. **(C).** Number of white blood cells (wbc) per gram of tissue and % of CD11b (+) and CD11c (+) stained cells in the stromal-vascular fraction of 4-month old aP2-*Ercc1*$^{F/-}$ and aP2-*Ercc1*$^{F/+}$ animals (as indicated). **(D).** Confocal imaging of whole-mount aP2-

Ercc1$^{F/-}$ WAT indicating the presence of MAC1(+) cells expressing pro-inflammatory molecules iNOS, CD45 and monocyte-attracting cell adhesion ICAM-1 and VCAM molecules in the CLS (as indicated). **(E).** Protein (left) and mRNA (right) levels of IL-6, TNFα and KC measured by whole-tissue ELISA and qPCR respectively in the WAT of 4-month old aP2-*Ercc1*$^{F/-}$ mice and aP2-*Ercc1*$^{F/+}$ controls. Scale bars: 20 μm, error bars indicate S.E.M. among replicates (n ≥ 3), p-value: *≤0.05, **≤0.01. See also Figure S4.

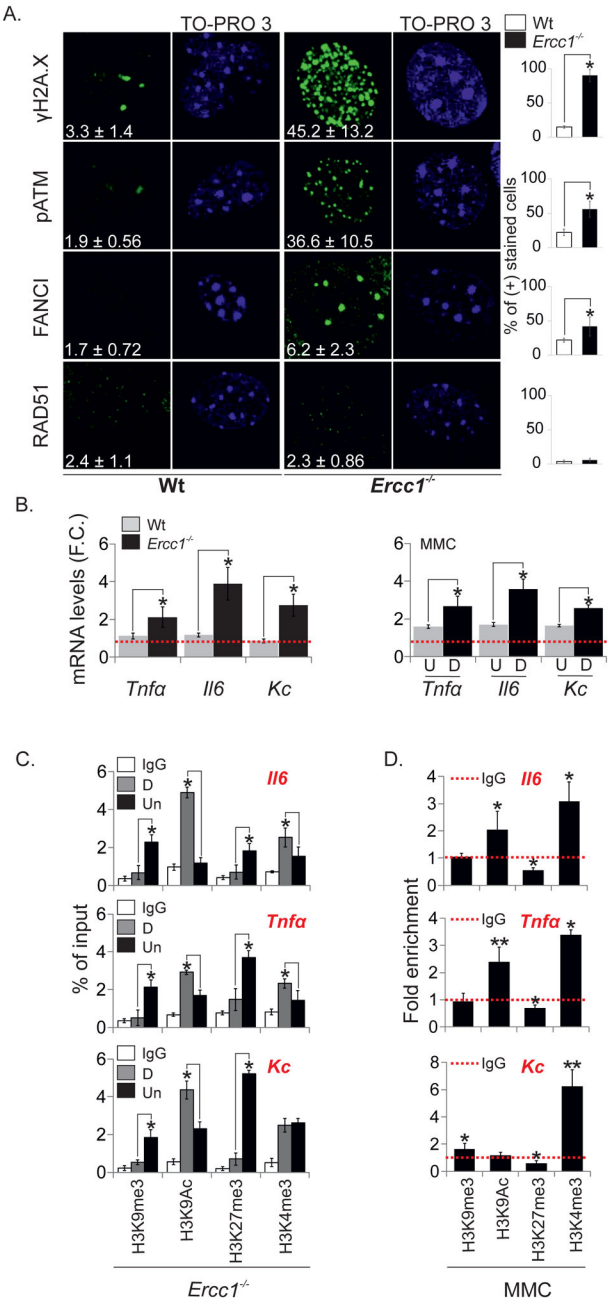

Figure 6. Accumulation of persistent DNA ICLs leads to histone PTMs associated with active transcription of pro-inflammatory cytokines

(A). Immunofluorescence detection of γH2A.X, pATM, FANCI and RAD51 proteins in wt and *Ercc1*$^{-/-}$ mouse embryonic fibroblasts (MEFs) exposed to the adipogenic stimulus (differentiated - D). Note the accumulation of γH2A.X, pATM and FANCI but not of RAD51 nuclear foci in *Ercc1*$^{-/-}$ adipocytes. The number at the bottom depicts the average number of foci per cell ± st. dev form 20 fields analysed from 3 or more cell cultures. **(B).** Quantitative (q) PCR mRNA levels of *Tnfa*, *Il6* and *Kc* pro-inflammatory cytokines in *Ercc1*$^{-/-}$ or wt adipocytes as compared to MEFs (left) and in mitomycin C (MMC)-treated wt adipocytes (D) or MEFs (U) as compared to non-MMC treated wt adipocytes or MEFs

respectively (right) **(C).** ChIP signals (shown as % of input) of repressive H3K9me3, H3K27me3, activating H3K9Ac, H3K4me3 histone marks and IgG control at the *Il6*, *Tnfa* and *Kc* proximal promoter regions in adipocytes or MEFs carrying the Ercc1 defect (*Ercc1*$^{-/-}$). Error bars indicate S.E.M. among replicates (n ≥ 3). P-value: *≤0.05. **(D).** ChIP signals (shown as fold enrichment) of repressive H3K9me3, H3K27me3 and activating H3K9Ac, H3K4me3 histone marks at the *Il6*, *Tnfa* and *Kc* proximal promoter regions in wt adipocytes exposed to MMC as compared to untreated controls. ChIP signals were normalized to input and expressed as fold enrichment over those obtained with control antibody (IgG), which were set as 1 (red dotted line). D: differentiated; U: undifferentiated. Error bars indicate S.E.M. among replicates (n ≥ 3). P-value: *≤0.05. See also Figure S5.

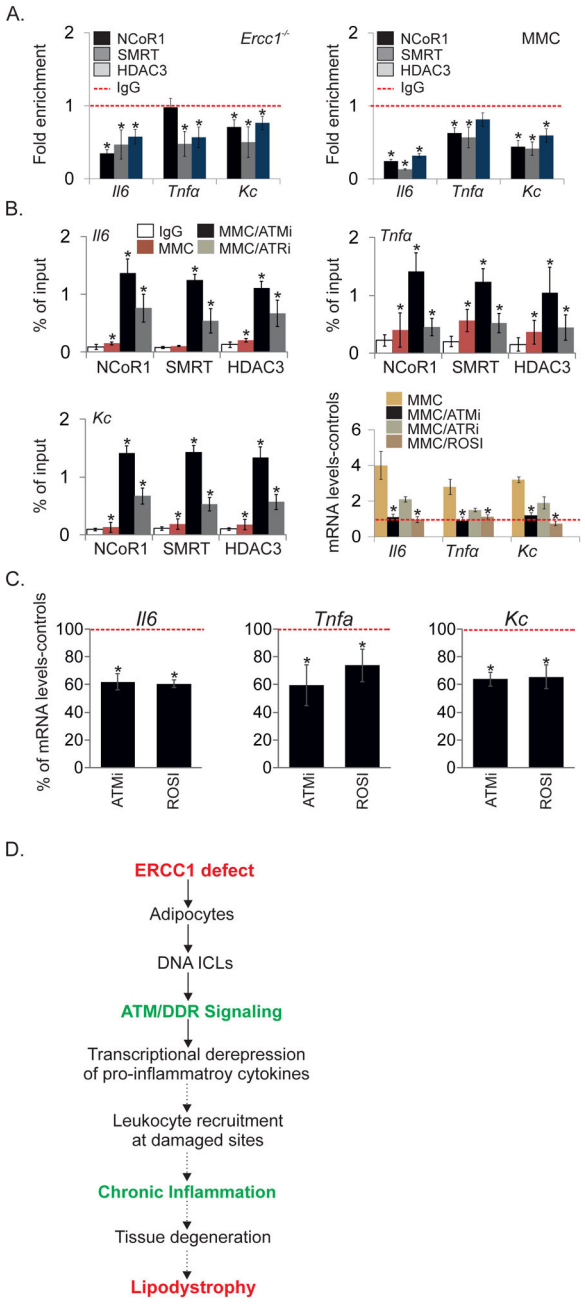

Figure 7. Persistent ICLs trigger the transcriptional de-repression of pro-inflammatory cytokines

(A). ChIP signals of the nuclear receptor co-repressors NCoR1, SMRT and HDAC3 on promoters of pro-inflammatory cytokines in *Ercc1*$^{-/-}$ adipocytes (shown in left) and wt MMC-treated adipocytes (right) as compared to corresponding, undifferentiated controls (n=3). ChIP signals were normalized to input and expressed as fold enrichment over those obtained with control antibody (IgG), which were set as 1 (red dotted line). P-value: *≤0.05**.** **(B).** ChIP signals of the nuclear receptor co-repressors NCoR1, SMRT, HDAC3 and IgG control on promoters of pro-inflammatory cytokines in wt MMC-treated adipocytes in the presence or absence of ATM (ATMi) and ATR (ATRi) kinase inhibitors (as shown). qPCR

mRNA levels of *Il6*, *Tnfα* and *Kc* in MMC-treated adipocytes exposed to the ATM (ATMi) and ATR (ATRi) kinase inhibitors (as shown). **(C).** qPCR mRNA levels of *Il6*, *Tnfα* and *Kc* in *Ercc1*$^{-/-}$ adipocytes exposed to ATM inhibitor (ATMi) and Rosiglidazone as compared to non-treated *Ercc1*$^{-/-}$ adipocytes (as shown). **(D).** Schematic representation of the causal relationship between the ERCC1 deficiency, persistent DDR signaling and adipose tissue degeneration in DNA repair-defective animals. Data are represented as mean ± SEM. See also Figure S5.